Metabolic Control of Viral Infection through PPAR-α Regulation of STING Signaling

Lili Tao[1], Alexandria Lowe[1], Guoxun Wang[1], Igor Dozmorov[1], Tyron Chang[1], Nan Yan[1,2], Tiffany A. Reese[1,2*]

[1]Department of Immunology, University of Texas Southwestern Medical Center, Dallas, TX, 75390, USA
[2]Department of Microbiology, University of Texas Southwestern Medical Center, Dallas, TX, 75390, USA

*corresponding author

Abstract

Cellular metabolic pathways contribute to many aspects of viral infection and may have pro-viral as well as antiviral functions. However, specific mechanisms for metabolic regulation of antiviral immunity are not well understood. Peroxisomes are essential sites of fatty acid metabolism and regulate immune signaling. We investigated the function of peroxisomal metabolism in herpesvirus infection and innate immunity *in vivo* and *ex vivo.* We found that induction of peroxisomal activity through the activation of the nuclear receptor PPAR-α enhanced herpesvirus replication. PPAR-α activation increased reactive oxygen species (ROS), which inhibited activation of stimulator of interferon (STING), a signaling molecule in the cytosolic DNA sensing pathway that induces antiviral type I interferon. Importantly, stimulation of peroxisomal activity in mice enhanced herpesvirus replication and pathogenesis comparable to levels observed previously in type I interferon receptor knockout mice. These findings are the first to indicate that peroxisomal lipid metabolism and ROS directly regulate immunity to cytoplasmic DNA.

Introduction

The metabolic machinery of the cell is a key component of host defense and immune cell function. Eukaryotic host cells adapt their cellular environments to enhance host defense

against invading viruses. Conversely, viruses evolve ways to manipulate host cell metabolism to promote virus replication.

Intermediates of cellular metabolism are important signaling molecules that alter immune defense pathways (O'Neill et al., 2016). For example, citrate and succinate from the tricarboxylic acid (TCA) cycle modify macrophage function by enhancing nitric oxide and cytokine production, respectively. The interrelatedness of immune cell function and metabolic pathways, including the TCA cycle, oxidative phosphorylation, and fatty acid oxidation have been comprehensively studied in mitochondria. However, peroxisomes, which are sites of lipid metabolism, also have the potential to modify immune cell function. Peroxisomes synthesize phospholipids and bile acids and oxidize very long, branched chain, and polyunsaturated fatty acids. As their name implies, peroxisomes produce significant amounts of hydrogen peroxide and other reactive oxygen species (ROS). ROS have been widely implicated in inflammatory processes, particularly for NFκB signaling and inflammasome activation (Forrester et al., 2018).

Peroxisomes are important sites of antiviral immunity. RIG-I-like receptors (RLRs) in the cytoplasm detect viral RNA and activate the adapter protein mitochondrial antiviral signaling protein (MAVS). MAVS is anchored on not only the outer mitochondrial membrane, but also on peroxisomes. Peroxisomal MAVS generates an early antiviral response that is unique from mitochondrial MAVS and independent of interferon-β (IFNβ) (Dixit et al., 2010). Certain RNA viruses, including flaviviruses, induce loss of peroxisomes and impaired antiviral immune responses (You et al., 2015). These data suggest that peroxisomes function in antiviral immunity to RNA viruses. However, it is unclear whether peroxisomes function in innate immunity to DNA viruses and cytoplasmic DNA.

Herpesviruses are enveloped DNA viruses that establish chronic infections in their hosts. After acute replication, herpesviruses enter a quiescent phase, termed latency, for the life of the host. Latency is characterized by limited viral gene expression and no viral progeny production.

However, latency is punctuated with brief periods of viral reactivation leading to viral progeny production and spread of the virus to new cells and hosts. In order to enter and maintain viral latency, herpesviruses must manipulate the cellular environment to favor viral persistence and evade immune recognition (Barton et al., 2011).

Peroxisomal proliferation is a notable feature of herpesvirus infection. The γ-herpesvirus Kaposi's sarcoma associated herpesvirus (KSHV), the α-herpesvirus Herpes simplex virus (HSV)-1, and the β-herpesvirus human cytomegalovirus (HCMV) all increase peroxisomes in infected cells (Beltran et al., 2018; Sychev et al., 2017). Moreover, each of these viruses encodes viral proteins (vFLIP for KSHV, vMIA for HCMV, and VP16 for HSV-1) that target peroxisomes, suggesting that modulation of peroxisomal function is important for the virus (Choi et al., 2018; Magalhães et al., 2016; Zheng and Su, 2017). A recent report found that HCMV and HSV-1 induced peroxisome biogenesis and plasmalogen production, leading to enhanced virus envelopment and lytic replication (Beltran et al., 2018). However, these data do not address the potential role of peroxisome biogenesis in chronic infection with a herpesvirus. KSHV latent cell survival requires peroxisomal lipid metabolism, suggesting that KSHV modulates peroxisomal lipid metabolism to support latent infection (Sychev et al., 2017).

In order to examine the role of peroxisome metabolism in herpesvirus infection *in vivo* we employed a murine model of γ-herpesvirus infection, murine gammaherpesvirus-68 (MHV68), to study the effect of peroxisomal activation on lytic and latent γ-herpesvirus infection. Similar to the human γ-herpesviruses, KSHV and Epstein Barr virus (EBV), this virus establishes latent infection in the host and reactivates in response to various immune and chemical signals (Barton et al., 2011; Reese, 2016; Reese et al., 2014). MHV68 also leads to lymphomas and tumors in immunocompromised hosts, similar to the human viruses (Barton et al., 2011).

Here we investigated the consequences of increased peroxisomal metabolism on herpesvirus infection and induction of antiviral immune responses. We induced peroxisomal

metabolism with fibrates, which are drugs used in humans to lower serum triglycerides levels (Staels et al., 1998). These drugs are agonists for peroxisome proliferator activated receptor (PPAR)-α, which is a member of a subfamily of nuclear hormone receptors that drive expression of genes involved in fatty acid oxidation (Issemann and Green, 1990; Reddy and Hashimoto, 2001). We discovered that activation of PPAR-α increased virus replication and inhibited type I interferon production following DNA-virus infection or direct stimulation of the cyclic GMP-AMP synthase (cGAS)/stimulator of interferon (STING) pathway. Importantly, treatment of mice with PPAR-α agonist led to increased herpesvirus replication, heightened lethality, and enhanced herpesvirus reactivation from latency in agonist-treated mice. Our data suggest that activation of PPAR-α suppresses cytoplasmic DNA sensing by generating high ROS that inhibit STING activation, leading to reduced type I interferon and impaired immunity to viral infections.

Results

Activation of PPAR-α promotes MHV68 replication.

To examine the effects of increased peroxisome biogenesis and fatty acid oxidation on herpesvirus infection, we treated macrophages with fibrates to stimulate peroxisome metabolism. Bone marrow derived macrophages were treated with PPAR-α agonists, fenofibrate or WY14643, and infected them with MHV68. Using a flow cytometric assay to determine the amount of lytic viral protein expressed on infected cells (Reese et al., 2014), we compared PPAR-α agonist treatment with agonists for two closely related nuclear receptors, PPAR-β/δ and PPAR-γ (GW501516 and rosiglitazone, respectively). We found that PPAR-α agonists fenofibrate and WY14643 both increased expression of lytic viral proteins on infected macrophages compared with untreated cells or cells treated with GW501516 or rosiglitazone (Figure 1A). MHV68 replication at either low or high multiplicity of infection (MOI) was also

increased in macrophages treated with fenofibrate or WY14643 compared with untreated cells (Figure 1B, C, Supplemental Figure 1). Treatment with agonist had no effect on virus replication in macrophages isolated from *Ppara*$^{-/-}$ mice, suggesting that PPAR-α is critical for agonist effects (Figure 1D). We tested whether stimulation of PPAR-α affected replication of a β-herpesvirus that also infects macrophages and found that replication of murine cytomegalovirus (MCMV) was also increased by PPAR-α agonist (Supplemental Figure 2). Thus, PPAR-α stimulation increases herpesvirus replication in a PPAR-α-dependent manner.

PPAR-α stimulation suppresses type I IFN production in a STING-dependent manner

To broadly assess the impact of PPAR-α agonist on cells infected with virus, we performed RNA sequencing analysis on macrophages infected with virus and treated with WY14643. Six hours after infection, uninfected/vehicle treated, MHV68+/vehicle treated, uninfected/WY14643 treated cells, and MHV68+/WY14643 treated macrophages were prepared for RNA-seq. Pathway analysis of differentially expressed genes revealed that virus infection in both vehicle-treated and WY14643-treated cells increased expression of interferon responsive genes, genes involved in inflammation, and NFκB pathway genes (Figure 2A, Supplemental Table 1). However, PPAR-α stimulation reduced the magnitude of upregulation in infected cells. Thus, PPAR-α stimulation attenuates the early antiviral response in infected cells.

To confirm the sequencing results, we quantified expression of a subset of interferon stimulated genes. We measured *Isg20*, *Isg15*, and *Cxcl10* and confirmed that expression of these genes is reduced in both uninfected and infected macrophages treated with WY14643 (Figure 2B). We also measured expression of *Ifnb* and found that expression is reduced after agonist treatment (Figure 2B). These data suggest that PPAR-α stimulation suppresses the interferon response at baseline and after viral infection.

Because of the suppression of the early antiviral response, we tested whether the effects of PPAR-α stimulation depended on the type I interferon response. To test this, we examined viral growth in wildtype and *Ifnar*$^{-/-}$ macrophages with and without agonist treatment. As expected, virus grew substantially more in *Ifnar*$^{-/-}$ cells compared with wildtype cells. PPAR-α stimulation did not further increase virus replication in the knockout cells (Supplemental Figure 3). Thus, PPAR-α stimulation effects depend on type I interferon.

MHV68 is a DNA virus that induces interferon downstream of the cGAS/STING pathway; therefore, we hypothesized that PPAR-α stimulation could antagonize the early induction of interferon after recognition of cytoplasmic DNA. Cytoplasmic DNA is sensed by cGAS, leading to activation of endoplasmic reticulum adapter molecule STING. STING phosphorylates TBK1 and IRF3, leading to transcription of IFNβ. IFNβ then signals through the type I IFN receptor to induce interferon stimulated gene expression and more IFNβ expression. To test if PPAR-α stimulation could suppress IFNβ induction after direct activation of STING, macrophages were treated with vehicle or agonist and stimulated with DMXAA, a murine agonist of STING. We found that PPAR-α stimulation suppressed IFNβ expression after DMXAA transfection (Figure 2C). As expected, the PPAR-γ and PPAR-δ agonists rosiglitazone and GW-501516 did not suppress IFNβ expression after DMXAA treatment (Supplemental Figure 4). Moreover, PPAR-α stimulation suppressed production of IFNβ protein (Figure 2D). These data suggest that PPAR-α stimulation antagonizes the induction of interferon production downstream of the STING DNA sensing pathway.

To test if suppression of IFNβ depended on STING, we treated *Sting*$^{-/-}$ macrophages with PPAR-α agonist and infected with MHV68. We found that PPAR-α stimulation no longer increased virus replication in cells deficient in STING (Figure 2E). We examined activation of TBK1 and IRF3 and found that PPAR-α stimulation suppressed DMXAA-induced phosphorylation of both proteins (Figure 2F). These data indicate that the effects of PPAR-α

agonist depend on STING expression and suggest that PPAR-α stimulation antagonizes the initial induction of IFNβ after recognition of cytoplasmic DNA.

PPAR-α stimulation induces oxidative stress

We wondered if PPAR-α agonist effects could promote virus replication even if cells were treated with agonist after infection, or if the effects of agonist required pretreatment. To test this, we compared three different treatment protocols. We pretreated, as above, with PPAR-α agonist overnight and replaced agonist in the media following infection with MHV68. We compared this with pretreatment only (pre) or post treatment only (post). We found that pretreatment with PPAR-α agonist was required to increase MHV68 replication (Figure 3A). We found no increase in virus replication when cells were treated post-infection with agonist. We also found that pretreatment alone was sufficient to increase virus replication. These data suggest that PPAR-α stimulation is altering the cellular environment prior to infection in such a way that enhances virus replication.

In order to determine how PPAR-α stimulation was altering the cellular environment to promote virus replication and impair interferon induction, we examined vehicle and WY14643-only treatments from our sequencing data. PPAR-α agonist treated cells displayed increased antioxidant response pathways, indicating a possible increase in oxidative stress in PPAR-α agonist treated cells (Figure 3B, Supplemental Table 2). To confirm these results, we analyzed expression of antioxidant genes in untreated or PPAR-α agonist treated macrophages and confirmed increased expression of *Mgst1*, *Gsr*, *Slc7a11*, *Gstm1*, *Gclm*, and *Cd36* in agonist treated cells (Figure 3C). PPAR-α agonist treatment of macrophages also promoted increase total ROS (Figure 3D). These results are comparable to previous data indicating that PPAR-α

agonist treatment increases β-oxidation of fatty acids in peroxisomes and enhances production of ROS (Reddy and Hashimoto, 2001; Teissier et al., 2004).

Given that PPAR-α stimulation increased antioxidant gene expression and ROS production and that these effects correlated with increased viral replication, we next tested whether increased ROS suppressed IFNβ production. Macrophages were treated with hydrogen peroxide (H_2O_2) and stimulated with DMXAA. H_2O_2 treatment suppressed DMXAA-induced IFNβ production (Figure 3E). In addition, N-Acetyl-L-cysteine (NAC), an antioxidant, partially neutralized the effects of H_2O_2 (Figure 3E). H_2O_2 treatment suppressed phosphorylation of TBK1 and IRF3 (Figure 3F). This indicates that increased oxidative stress suppresses the cGAS/STING pathway after activation with cytoplasmic DNA.

To determine if cells that have constitutive high levels of ROS have impaired interferon responses, we examined that antiviral response in nuclear factor E2-related factor 2 (NRF2) deficient cells. NRF2 is a transcription factor that regulates antioxidant responses by binding to antioxidant response elements (ARE) found in promoters of detoxication enzymes. NRF2 activity is regulated by KEAP1, and KEAP1 under non-stressed conditions promotes NRF2 ubiquitylation. When cells are under oxidative stress, NRF2 is released from KEAP1 and drives antioxidant gene expression (Nguyen et al., 2009). *Nrf2*$^{-/-}$ cells do not induce antioxidant genes and have high levels of ROS (Chan et al., 1996; Itoh et al., 1997; McMahon et al., 2001). We confirmed that *Nrf2*$^{-/-}$ macrophages had increased ROS (Figure 3G). When we stimulated *Nrf2*$^{-/-}$ macrophages with DMXAA they induced less *Ifnb* expression compared to wildtype cells (Figure 3H). Additionally, PPAR-α agonists did not further suppress *Ifnb* transcript production from knockout cells (Figure 3H). Together, these data suggest that ROS can suppress IFNβ downstream of direct STING activation.

To determine if the lower levels of IFNβ expressed in *Nrf2*$^{-/-}$ macrophages led to increased viral replication, we infected *Nrf2*$^{-/-}$ and wildtype macrophages with MHV68. We

observed increase viral protein expression after infection in *Nrf2*$^{-/-}$ macrophages, indicating that virus replicated better in cells with higher levels of ROS and decreased IFNβ (Figure 3I).

PPAR-α stimulation increases virus replication and lethality in mice.

Because we found that PPAR-α stimulation *in vitro* suppressed interferon production, we hypothesized that agonist treatment of mice infected with MHV68 would alter herpesvirus replication. Previously published work established that mice deficient in the IFNα/β receptor (IFNAR) have increased viral replication and enhanced susceptibility to MHV68 (Dutia et al.). To determine if PPAR-α stimulation increased MHV68 replication *in vivo,* we injected wildtype and *Ppara*$^{-/-}$ mice with WY14643 or vehicle control for 7 days, starting 3 days prior to infection and continuing for 4 days after infection (Figure 4A). Mice were infected with a dose of MHV68 that does not cause lethality in wildtype mice treated with the drug vehicle. However, wildtype mice injected with PPAR-α agonist succumbed to infection (Figure 4B), at a frequency similar to type I interferon receptor deficient mice (Dutia et al.). Moreover, *Ppara*$^{-/-}$ mice treated with agonist or vehicle all survived infection with MHV68, indicating that the lethality observed in wildtype mice treated with agonist is PPAR-α dependent (Figure 4C). Using a luciferase-tagged MHV68 (MHV68-M3FL) we imaged mice infected with virus over multiple days during acute infection (Hwang et al., 2008; Reese et al., 2014). We found that mice treated with WY14643 had increased virus replication compared to vehicle treated mice, and that this increase in virus replication was PPAR-α dependent (Figure 4D, E). These data suggest that PPAR-α stimulation significantly increased MHV68 acute replication.

To determine if the interferon response was altered by PPAR-α stimulation, we analyzed interferon stimulated gene expression in the peritoneal cells for vehicle-treated and agonist-treated mice. We found that expression of *Isg20* and *Cxcl10* was decreased in agonist treated

mice (Figure 4F), indicated that treatment with PPAR-α agonist during acute infection suppressed the interferon response.

PPAR-α stimulation induces herpesvirus reactivation.

We hypothesized that if PPAR-α stimulation induces ROS and impairs the production of interferon, then PPAR-α agonist may enhance MHV68 reactivation from latency. Previous work demonstrated increased reactivation from latency in mice deficient in IFNAR or in mice that received a blocking antibody for IFNAR (Barton et al., 2005; Steed et al., 2006). Additionally, oxidative stress induces KSHV reactivation from latency in cell lines (Li et al., 2011; Ye et al., 2011). We examined PPAR-α expression in latently infected spleens and peritoneal exudate cells (PECs) and found that latent virus infection induced PPAR-α expression (Figure 5A). To determine if PPAR-α stimulation could increase virus reactivation, we infected mice with MHV68-M3FL and waited for one month to establish latency prior to treatment with WY14643 (Figure 5B). By this time there is little to no luciferase expression from the virus, indicating that the virus is quiescent (Hwang et al., 2008; Reese et al., 2014). Upon virus reactivation, luciferase is expressed and quantitated with an *in vivo* bioluminescence reader. When mice were treated with vehicle control or WY14643 alone there was no measurable virus reactivation (Figure 5C). However, we found previously that reactivation of MHV68 requires 2 signals (Reese et al., 2014). Neither administration of IL-4, a direct inducer of herpesvirus latent-to-lytic gene expression, nor administration of a blocking antibody to IFNγ, a suppressor of virus reactivation, was sufficient to induce MHV68 reactivation. However, the combination of IL-4 and anti-IFNγ treatment induced significant virus reactivation. Therefore, we hypothesized that if PPAR-α agonist was suppressing type I IFN, then a positive inducer of herpesvirus gene expression may be required to promote MHV68 reactivation. To test this, we combined

WY14643 with long-lasting IL-4 complexes (IL-4c). When compared to IL-4c alone, WY14643 alone, or vehicle the combination of WY14643 and IL-4c induced significant virus reactivation from latency (Figure 5C, D). Thus, PPAR-α stimulation induces herpesvirus reactivation from latency.

Discussion

We determined that induction of peroxisome metabolism and β-oxidation of fatty acids by PPAR-α agonist increases virus replication and reactivation. In macrophages, PPAR-α stimulation increased virus replication and suppressed the induction of an interferon response in a STING-dependent manner. PPAR-α stimulation induced oxidative stress in cells and high levels of oxidative stress impaired STING-induced interferon production. This is the first evidence that PPAR-α activation and peroxisomal metabolism regulate the cytoplasmic DNA-sensing pathway and IFNβ production downstream of STING. PPAR-α stimulation significantly increased herpesvirus replication in mice, leading to increased lethality of agonist-treated mice. Not only did PPAR-α stimulation increase herpesvirus acute replication, but PPAR-α agonist also increased MHV68 reactivation from latency in combination with IL-4 treatment. These data are the first to indicate that, during latency, peroxisomes modulate interferon production. Peroxisomal metabolism may represent a strategy used by herpesviruses to fine-tune interferon production for the purposes of modulating virus latency and reactivation.

Metabolism is recognized as an important regulator of immunity. Metabolic reprogramming of macrophages, in particular, is essential for modifying their inflammatory phenotype and function. Glycolysis drives inflammatory macrophage responses, whereas high fatty acid oxidation was long thought to support anti-inflammatory macrophage responses (den Bossche et al., 2017). It is now clear that fatty acid oxidation is not just anti-inflammatory,

because oxidation of palmitate promotes the production of mitochondrial ROS, which induces inflammasome activation (Hall et al., 2013; Moon et al., 2016). Moreover, mitochondrial ROS promotes the production of the proinflammatory cytokines IL-1β, IL-6, and TNFα following LPS stimulation of macrophages (Bulua et al., 2011). Our data adds another level of complexity to the role of ROS in inflammation. Peroxisomes are essential for the metabolism of very long chain fatty acids and they produce significant quantities of ROS. Our data indicates that ROS, perhaps derived from peroxisomal β-oxidation of very long chain fatty acids, impairs STING activation and interferon production. Further work is needed to determine the source of ROS. However, our data thus far suggests that the induction of peroxisomal metabolism and fatty acid oxidation, leading to high ROS production, alters innate immune signaling.

These data reveal that peroxisomal metabolism and increased ROS production regulates the cytoplasmic DNA sensing pathway. Previously, the adapter molecule MAVS that signals downstream of RNA recognition was found localized to not only mitochondria, but also peroxisomes. Interestingly, the peroxisomal localization of MAVS dictates unique signaling pathways and gene responses distinct from mitochondrial MAVS (Dixit et al., 2010; Odendall et al., 2014). Together these data along with our data indicate that peroxisomes are critical organelles for the induction of innate immune signals, either through localization of critical signaling molecules or production of metabolites that regulate immune signaling.

Herpesviruses use multiple mechanisms to maintain latency in the host and peroxisomal metabolism is a putative novel mechanism. To avoid clearance, herpesviruses evade immune recognition by downregulating antigen presentation, expressing viral proteins that regulate the interferon pathway, inhibiting cell cycle arrest and apoptosis, and encoding various molecular mimics. This is indicative of a long evolutionary relationship with the host. It also suggests that herpesviruses modify numerous pathways within the host cell to tune the balance between latency and reactivation. Peroxisomal proliferation is a feature of herpesvirus infection, but the

function of peroxisomal biogenesis during latency has been elusive. We show that PPAR-α expression is increased during herpesvirus latency, and that peroxisomal metabolism suppresses interferon production, leading to viral reactivation from latency. This suggests that peroxisomes and the redox balance of the cell may regulate latency by adjusting the production of type I interferon.

A key remaining question is how ROS regulates STING activation. Recent structural data provide numerous insights into the mechanism of cGAMP activation of STING (Ergun et al., 2019; Shang et al., 2019). STING dimers in the ER form polymers upon binding to cGAMP and disulfide bonds in the cytosolic domain stabilize STING polymers. These inter-dimer crosslinks are important for STING activation. One possibility is that increased oxidative stress leads to oxidation of cysteine residues in the cytosolic domain, which interferes with the polymerization and activation of STING.

Overall, our work suggests that metabolism and particularly ROS have both proinflammatory and anti-inflammatory functions. These results have implications for therapies that induce or suppress oxidative stress, either for the treatment of infection, cancer or autoimmune disease.

Acknowledgments

We thank members of the Reese and Yan labs for technical assistance, David Mangelsdorf and Steven Kleiwer for reagents and expertise, Dr. Wenhan Zhu for help with data analysis, and Drs. Julie Pfeiffer and Lora Hooper for editorial assistance. We also thank the UTSW Flow Cytometry core and the Genomic and Microarray core for technical assistance. The Reese lab is supported by the American Heart Association (17SDG33670071), the NIH (1R01AI130020-01A1), and the Pew Scholars Program.

Author Contributions

L.T. performed and analyzed experiments, with technical assistance from A.L, G.W and T.C. I.D. performed RNAseq analysis. N.Y. provided reagents and expertise. T.A.R. directed the project and wrote the manuscript.

Declaration of Interests

The authors declare no competing interests.

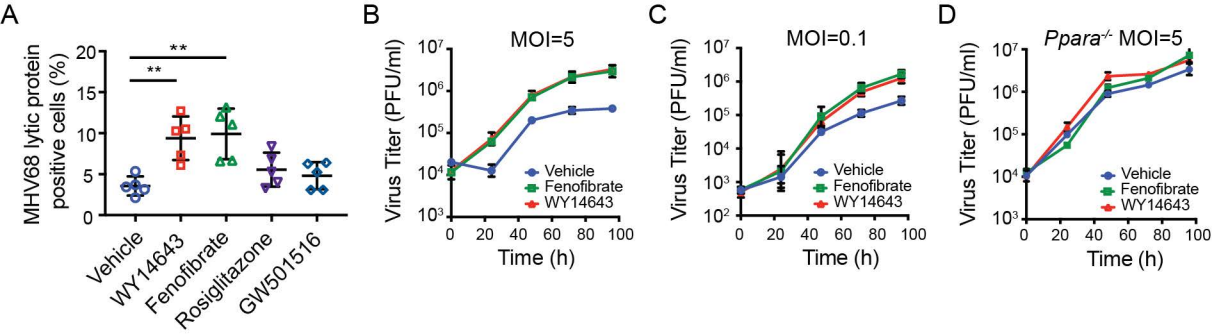
A
MHV68 lytic protein positive cells (%)
20
15
10
5
0
**
**
Vehicle
WY14643
Fenofibrate
Rosiglitazone
GW501516
B
MOI=5
Virus Titer (PFU/ml)
Time (h)
Vehicle
Fenofibrate
WY14643
C
MOI=0.1
Virus Titer (PFU/ml)
Time (h)
Vehicle
Fenofibrate
WY14643
D
Ppara-/- MOI=5
Virus Titer (PFU/ml)
Time (h)
Vehicle
Fenofibrate
WY14643

Figure 1. PPAR-α stimulation increases MHV68 replication.

(A) Macrophages from C57BL6/J mice were pretreated for 16 hours with WY14643, fenofibrate, rosiglitazone, or GW501516. Cells were infected with MHV68 at MOI=5. Quantification of cells expressing MHV68 lytic proteins using a polyclonal antibody 24 hours after infection was measured by flow cytometry. Data represents mean ± SD from 5 independent experimental.

(B-C) Growth curve of MHV68 in macrophages isolated from C57BL/6J mice after pretreatment with vehicle, WY14643 or fenofibrate. Cells were infected with MHV68 at MOI=5 (B) or MOI=0.1 (C). Virus quantitated by plaque assay on 3T12 cells. Data represents mean ± SD from 3 independent experiments.

(D) Growth curve of MHV68 in macrophages isolated from *Ppara*$^{-/-}$ mice after pretreatment with vehicle, WY14643 or fenofibrate. Cells were infected with MHV68 at MOI=5. Data represents mean ± SD from 3 independent experiments.

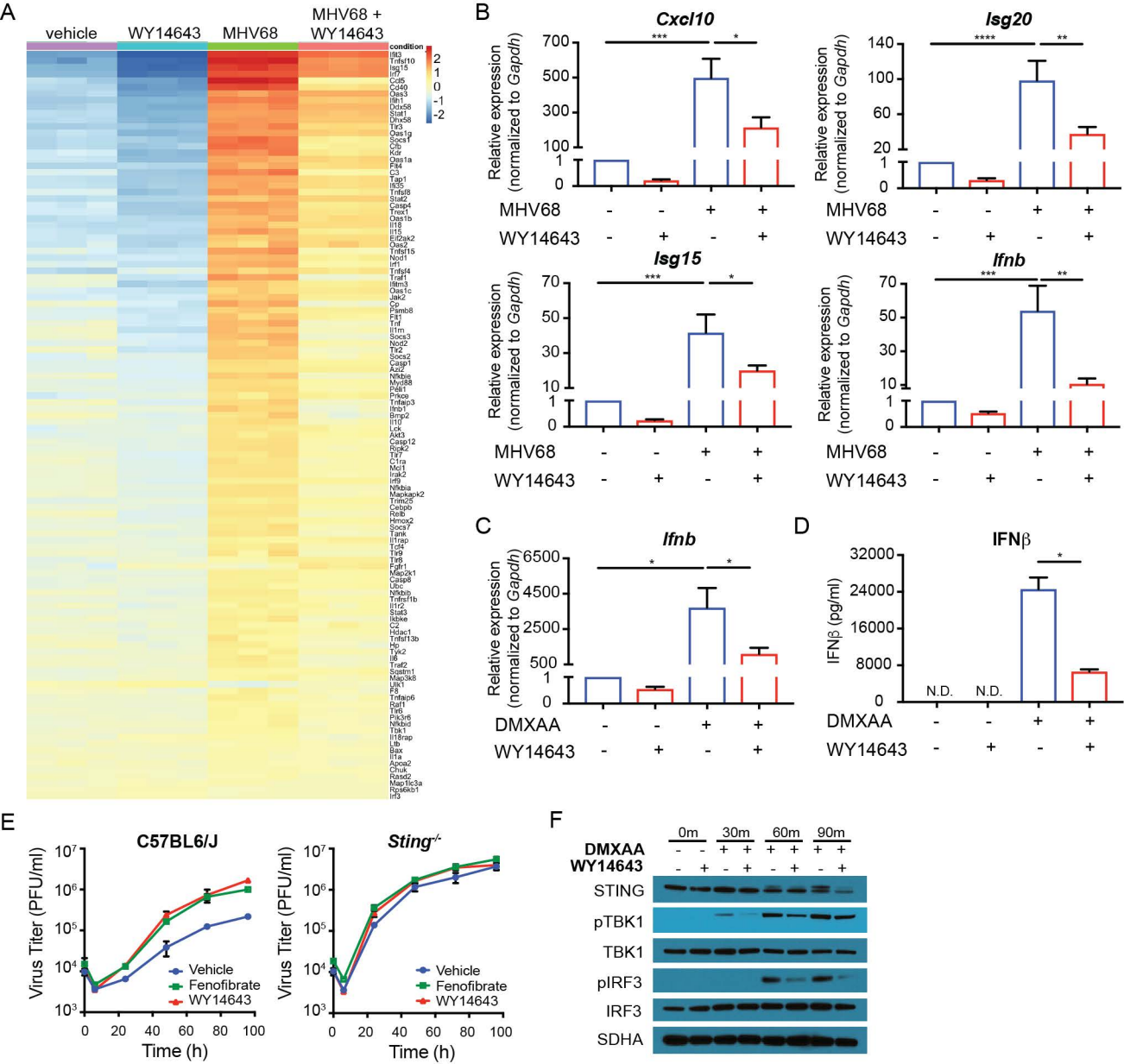
A
vehicle
WY14643
MHV68
MHV68 + WY14643
condition
2
1
0
-1
-2
B
Cxcl10
Isg20
Isg15
Ifnb
Relative expression (normalized to Gapdh)
MHV68
WY14643
C
Ifnb
DMXAA
D
IFNβ
IFNβ (pg/ml)
N.D.
E
C57BL6/J
Sting-/-
Virus Titer (PFU/ml)
Time (h)
Vehicle
Fenofibrate
WY14643
F
0m
30m
60m
90m
DMXAA
WY14643
STING
pTBK1
TBK1
pIRF3
IRF3
SDHA

Figure 2. PPAR-α stimulation suppresses type I IFN in a STING-dependent manner.

(A) Macrophages were pretreated with vehicle or WY14643 for 16 hours prior to infection with MHV68, MOI=5. 6 hours after infection, RNA was isolated and prepared for RNA sequencing.

(B) Macrophages were pretreated with vehicle or WY14643 for 16 hours prior to infection with MHV68. qRT-PCR of *Cxcl10*, *Isg20*, *Isg15* and *Ifnb* before and 6 hours after MHV68 infection. Relative expression normalized to *Gapdh*. n=5 for *cxcl10*, n=7 for *Isg20*, n=6 for *Isg15*, n=8 for *Ifnb.*

(C) Macrophages were pretreated with vehicle or WY14643 for 16 hours prior to transfection with DMXAA. qRT-PCR of *Ifnb* before and 2 hours after transfection with DMXAA. Relative expression normalized to *Gapdh*. n=9.

(D) Macrophages were pretreated with vehicle or WY14643 for 16 hours prior to transfection with DMXAA. Concentration of IFNβ in culture medium before and 24 hours after transfection was determined by ELISA assay. n=3.

(E) Macrophages from C57BL6/J or *Sting*$^{-/-}$ mice were pretreated with vehicle or WY14643 for 16 hours prior to infection with MHV68, MOI=5. Virus growth was quantitated by plaque assay. n=3.

(F) Macrophages were pretreated with vehicle or WY14643 for 16 hours. Representative western blot of proteins involved in STING signaling before transfection and 30 mins, 60 mins, 90 mins after transfection with DMXAA.

Data all shown as mean ± SD; $^{*}p<0.05$, $^{**}p<0.01$, $^{***}P<0.001$, statistical analysis was conducted using one-way ANOVA test.

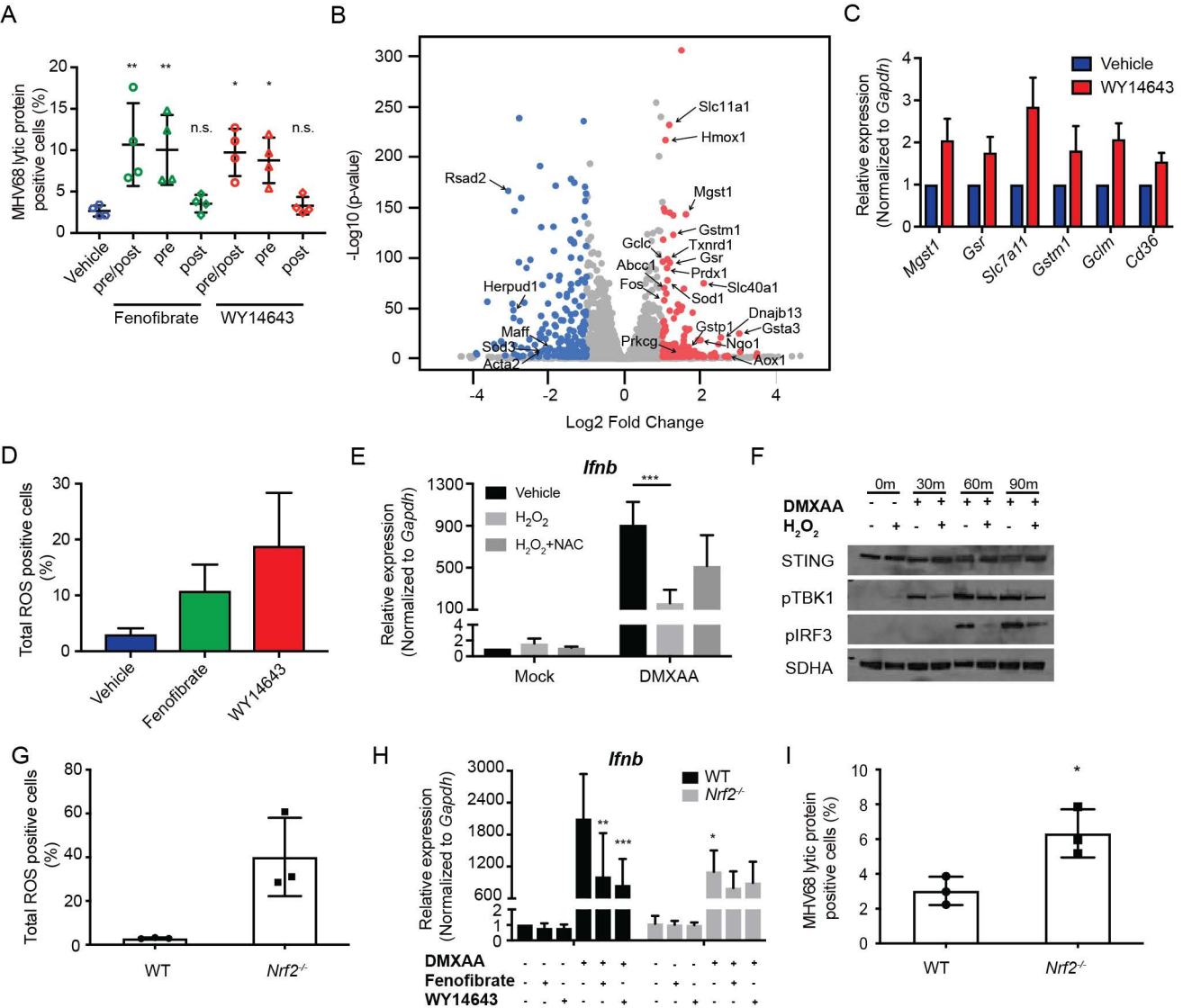
A
MHV68 lytic protein positive cells (%)
Vehicle
pre/post
pre
post
pre/post
pre
post
Fenofibrate
WY14643
n.s.
B
-Log10 (p-value)
Log2 Fold Change
Slc11a1
Hmox1
Rsad2
Mgst1
Gstm1
Gclc
Txnrd1
Gsr
Abcc1
Prdx1
Herpud1
Fos
Slc40a1
Sod1
Dnajb13
Gsta3
Gstp1
Maff
Prkcg
Ngo1
Sod3
Acta2
Aox1
C
Relative expression (Normalized to Gapdh)
Vehicle
WY14643
Mgst1
Gsr
Slc7a11
Gstm1
Gclm
Cd36
D
Total ROS positive cells (%)
Vehicle
Fenofibrate
WY14643
E
Ifnb
Relative expression (Normalized to Gapdh)
Vehicle
H2O2
H2O2+NAC
Mock
DMXAA
F
0m
30m
60m
90m
DMXAA
H2O2
STING
pTBK1
pIRF3
SDHA
G
Total ROS positive cells (%)
WT
Nrf2-/-
H
Ifnb
Relative expression (Normalized to Gapdh)
WT
Nrf2-/-
DMXAA
Fenofibrate
WY14643
I
MHV68 lytic protein positive cells (%)
WT
Nrf2-/-

Figure 3. Oxidative stress inhibits STING activation and interferon production.

(A) Macrophages were treated with vehicle, WY14643 or fenofibrate agonist pre and post-infection (pre/post), pre-infection only (pre) or post-infection only (post). Quantification of cells expressing MHV68 lytic proteins by FACs assay 24 hours after infection. n=4.

(B) Comparison of vehicle-treated or WY14643-treated macrophages from RNA sequencing analysis in Figure 2A.

(C) Macrophages were treated with either vehicle control or WY14643 overnight. Genes associated with oxidative stress response were quantitated by qRT-PCR. Relative expression normalized to *Gapdh*. n=5 from independent experiments.

(D) Macrophages were treated with vehicle, fenofibrate or WY14643 for 6 hours. Quantification of total ROS in BMDMs by flow cytometry. n=7 with vehicle and fenofibrate treatment, n=6 with WY14643 treatment.

(E) Macrophages were pretreated with vehicle control or H_2O_2 for 20 mins. Half of the H_2O_2 samples were treated with NAC for 30 minutes and half were mock treated. Treatments were replaced with fresh media and cells were transfected with DMXAA. After 2 hours *Ifnb* was quantitated from lysates by qRT-PCR. n=4 from independent experiments.

(F) Macrophages were treated with either vehicle or H_2O_2 for 20 mins, and then transfected with DMXAA. Expression of STING, phosphorylated TBK1 (pTBK1), phosphorylated IRF3 (pIRF3), and SDHA was quantitated 0, 30, 60 or 90 minutes after transfection. Representative of 3 separate experiments.

(G) Macrophages were isolated from C57BL6/J or *Nrf2*$^{-/-}$ mice. Total ROS was quantitated by flow cytometry. n=3 from independent experiments.

(H) Macrophages isolated from WT or *Nrf2*$^{-/-}$ mice were pretreated for 16 hours with fenofibrate, WY14643, or vehicle. Cells were transfected with DMXAA and expression of *Ifnb* transcript was quantitated 2 hours later. Relative expression of *Ifnb* was normalized to *Gapdh*. n=5

Data all shown as mean ± SD; $^{*}p<0.05$, $^{**}p<0.01$, $^{***}P<0.001$, statistical analysis was conducted using one-way ANOVA or two-way ANOVA test.

(I) Macrophages isolated from WT or *Nrf2*$^{-/-}$ mice were infected with MHV68 at a MOI=5 for 24 hours. Cells expressing MHV68 lytic proteins were quantified by FACs assay. N=3 from independent experiments.

Data all shown as mean ± SD; $^{*}p<0.05$, $^{**}p<0.01$, statistical analysis was conducted using one-way ANOVA or unpaired t-test.

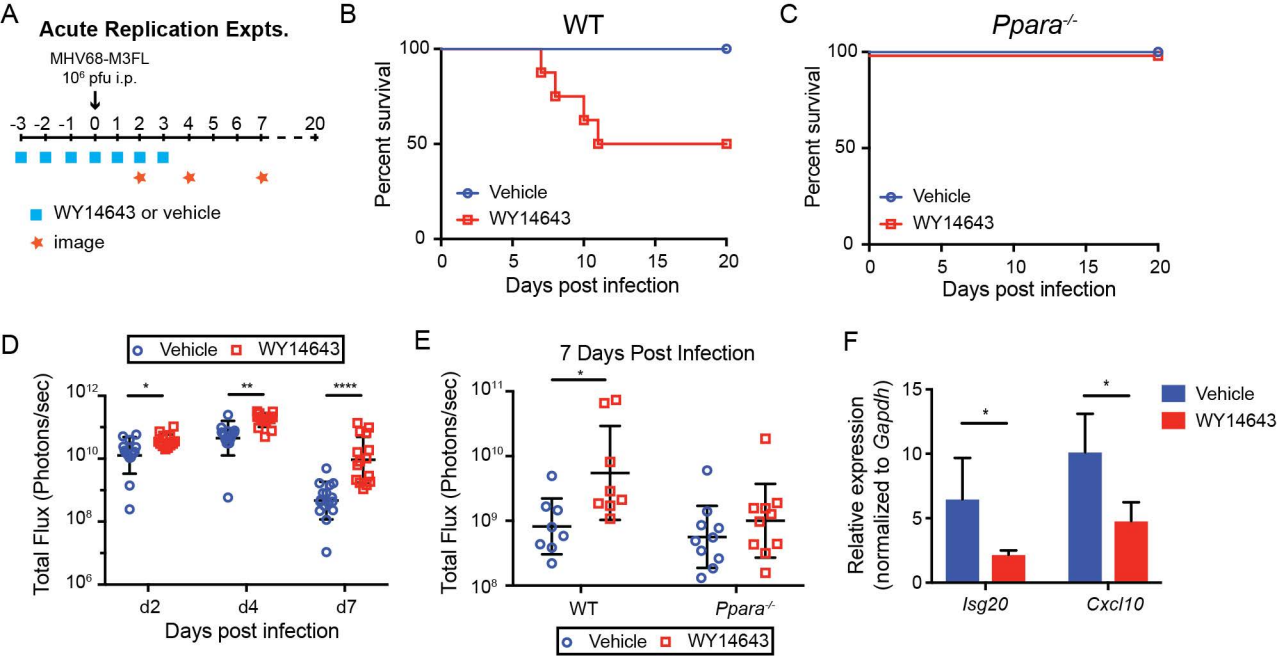
A
Acute Replication Expts.
MHV68-M3FL
10⁶ pfu i.p.
-3 -2 -1 0 1 2 3 4 5 6 7 20
WY14643 or vehicle
image
B
WT
Percent survival
Days post infection
Vehicle
WY14643
C
Ppara-/-
Percent survival
Days post infection
Vehicle
WY14643
D
Vehicle
WY14643
Total Flux (Photons/sec)
d2
d4
d7
Days post infection
E
7 Days Post Infection
Total Flux (Photons/sec)
WT
Ppara-/-
Vehicle
WY14643
F
Relative expression (normalized to Gapdh)
Isg20
Cxcl10
Vehicle
WY14643

Figure 4. PPAR-α stimulation in mice increases virus replication and lethality.

(A) Schematic for acute replication of MHV68 in mice. Mice were treated with either vehicle control (15% HS15) or WY14643 (100 mg/kg) for 7 days, starting 3 days before infection. Mice were infected intraperitoneally with MHV68-M3FL at dose of 10^6 PFU. Acute replication of virus was measured at d2, d4 and d7 after infection using an IVIS bioluminescent imager. Survival of mice was monitored until 20 days after infection.

(B-C) Survival of mice infected with MHV68. C57BL6/J (B) or *Ppara*$^{-/-}$ (C) mice were treated with either vehicle control or WY14643, and infected with MHV68. n=8 in each group of C57BL6/J mice, n=10 in each group of *Ppara*$^{-/-}$ mice. Data shown as the pool of 2 independent experiments.

(D) Acute replication of MHV68 in mice measured by luminescent intensity. n=16 in vehicle treatment group, n=15 in WY14643 treatment group, data shown as the pool of 3 independent experiments.

(E) Acute replication of MHV68 in WT or *Ppara*$^{-/-}$ mice measured by luminescent intensity. n=8 in each group of WT mice, n=10 in each group of *Ppara*$^{-/-}$ mice. Data shown as the pool of 2 independent experiments.

(F) Peritoneal exudate cells were collected from vehicle or WY14643-treated mice 2 days after infection with MHV68. Relative expression of *Isg20* and *Cxcl10* was quantitated and normalized to *Gapdh*. n=4 from 2 independent experiments.

Data all shown as mean ± SD; $^{*}p<0.05$, $^{**}p<0.01$, $^{***}P<0.001$, statistical analysis was conducted using one-way ANOVA or two-way repeated measures ANOVA test.

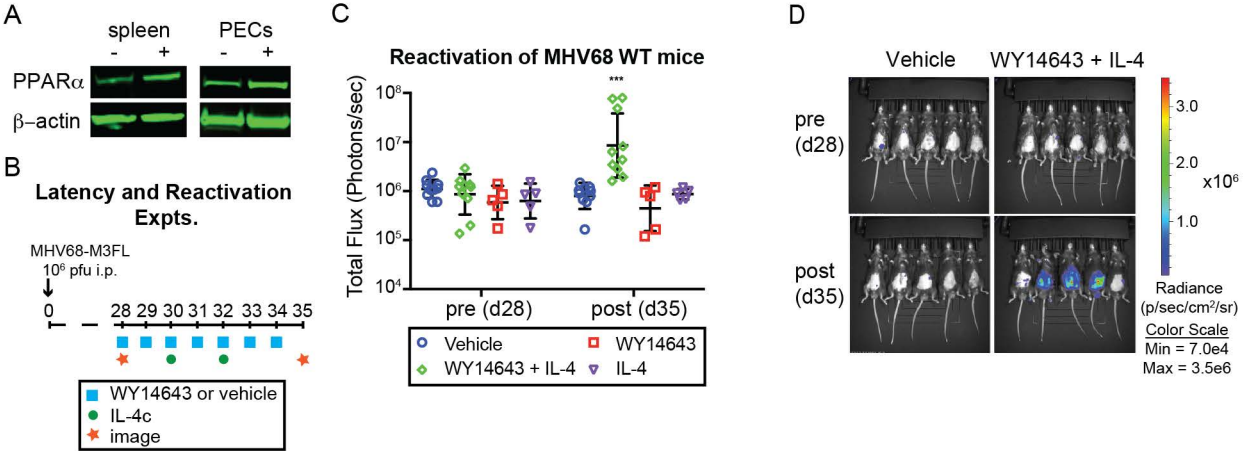
A
spleen
PECs
- +
- +
PPARα
β–actin
B
Latency and Reactivation Expts.
MHV68-M3FL
10⁶ pfu i.p.
0
28 29 30 31 32 33 34 35
WY14643 or vehicle
IL-4c
image
C
Reactivation of MHV68 WT mice
Total Flux (Photons/sec)
10⁸
10⁷
10⁶
10⁵
10⁴
***
pre (d28)
post (d35)
Vehicle
WY14643
WY14643 + IL-4
IL-4
D
Vehicle
WY14643 + IL-4
pre (d28)
post (d35)
3.0
2.0
1.0
x10⁶
Radiance (p/sec/cm²/sr)
Color Scale
Min = 7.0e4
Max = 3.5e6

Figure 5. PPAR-α stimulation induces herpesvirus reactivation.

(A) Spleen and PECs were collected from uninfected or day 28 MHV68-infected mice for analysis of PPAR-α and β-actin protein expression. Representative of 3 independent experiments.

(B) Schematic for MHV68 latency and reactivation experiments in mice. Mice were infected with MHV68-M3FL at the dose of 10^6 PFU, intraperitoneally. 4 weeks after infection, mice were treated with vehicle control, WY14643+IL-4c, WY14643 only or IL-4c only. Reactivation of MHV68 was quantified by imaging with an IVIS bioluminescent imager either prior to injection with treatments (d28, pre) or after treatments (d35, post).

(C) Quantification of luminescent intensity pre and post treatment with vehicle control, WY14643+IL-4c, WY14643 only or IL-4c only. n=10 in vehicle group and WY14643+IL-4c group; n=5 in WY14643-only and IL-4c-only group. Data shown as pool of 3 independent experiments.

(D) Luminescent intensity of 5 representative mice from vehicle or WY14643 + IL-4c treated groups pre and post treatment.

Data all shown as mean ± SD; $^{***}P<0.001$, statistical analysis was conducted using two-way repeated measures ANOVA test.

References

Barton, E., Mandal, P., and Speck, S.H. (2011). Pathogenesis and host control of gammaherpesviruses: lessons from the mouse. Annual review of immunology *29*, 351–397.

Barton, E.S., Lutzke, M.L., Rochford, R., and Virgin, H.W. (2005). Alpha/beta interferons regulate murine gammaherpesvirus latent gene expression and reactivation from latency. Journal of virology *79*, 14149–14160.

Beltran, P.M., Cook, K.C., Hashimoto, Y., Galitzine, C., Murray, L.A., Vitek, O., and Cristea, I.M. (2018). Infection-Induced Peroxisome Biogenesis Is a Metabolic Strategy for Herpesvirus Replication. Cell Host & Microbe *24*, 526-541.e7.

den Bossche, J., O'Neill, L.A., and Menon, D. (2017). Macrophage Immunometabolism: Where Are We (Going)? Trends in Immunology *38*, 395–406.

Bulua, A.C., Simon, A., Maddipati, R., Pelletier, M., Park, H., Kim, K.-Y.Y., Sack, M.N., Kastner, D.L., and egel, R. (2011). Mitochondrial reactive oxygen species promote production of proinflammatory cytokines and are elevated in TNFR1-associated periodic syndrome (TRAPS). The Journal of Experimental Medicine *208*, 519–533.

Chan, K., Lu, R., Chang, J., and Kan, Y. (1996). NRF2, a member of the NFE2 family of transcription factors, is not essential for murine erythropoiesis, growth, and development. Proceedings of the National Academy of Sciences of the United States of America *93*, 13943–13948.

Choi, Y.B., Choi, Y., and Harhaj, E.W. (2018). Peroxisomes support human herpesvirus 8 latency by stabilizing the viral oncogenic protein vFLIP via the MAVS-TRAF complex. PLoS Pathogens *14*, e1007058.

Dixit, E., Boulant, S., Zhang, Y., Lee, A.S., Odendall, C., Shum, B., Hacohen, N., Chen, Z.J., Whelan, S.P., Fransen, M., et al. (2010). Peroxisomes are signaling platforms for antiviral innate immunity. Cell *141*, 668–681.

Dutia, B., Allen, D., Dyson, H., and Nash, A. Type I interferons and IRF-1 play a critical role in the control of a gammaherpesvirus infection. Virology *261*, 173–179.

Ergun, S.L., Fernandez, D., Weiss, T.M., and Li, L. (2019). STING Polymer Structure Reveals Mechanisms for Activation, Hyperactivation, and Inhibition. Cell *178*, 290-301.e10.

Hall, C.J., Boyle, R.H., Astin, J.W., Flores, M.V., Oehlers, S.H., Sanderson, L.E., Ellett, F., Lieschke, G.J., Crosier, K.E., and Crosier, P.S. (2013). Immunoresponsive gene 1 augments bactericidal activity of macrophage-lineage cells by regulating β-oxidation-dependent mitochondrial ROS production. Cell Metabolism *18*, 265–278.

Hwang, S., Wu, T.-T., Tong, L.M., Kim, K., Martinez-Guzman, D., Colantonio, A.D., Uittenbogaart, C.H., and Sun, R. (2008). Persistent gammaherpesvirus replication and dynamic interaction with the host in vivo. Journal of virology *82*, 12498–12509.

Issemann, I., and Green, S. (1990). Activation of a member of the steroid hormone receptor

superfamily by peroxisome proliferators. Nature *347*, 645–650.

Itoh, K., Chiba, T., Takahashi, S., Ishii, T., Igarashi, K., Katoh, Y., Oyake, T., Hayashi, N., Satoh, K., Hatayama, I., et al. (1997). An Nrf2/small Maf heterodimer mediates the induction of phase II detoxifying enzyme genes through antioxidant response elements. Biochemical and Biophysical Research Communications *236*, 313–322.

Li, X., Feng, J., and Sun, R. (2011). Oxidative stress induces reactivation of Kaposi's sarcoma-associated herpesvirus and death of primary effusion lymphoma cells. Journal of virology *85*, 715–724.

Magalhães, A.C., Ferreira, A.R., Gomes, S., Vieira, M., Gouveia, A., Valença, I., Islinger, M., Nascimento, R., Schrader, M., Kagan, J.C., et al. (2016). Peroxisomes are platforms for cytomegalovirus' evasion from the cellular immune response. Scientific Reports *6*, 26028.

McMahon, M., Itoh, K., Yamamoto, M., Chanas, S., Henderson, C., McLellan, L., Wolf, C., Cavin, C., and Hayes, J. (2001). The Cap'n'Collar basic leucine zipper transcription factor Nrf2 (NF-E2 p45-related factor 2) controls both constitutive and inducible expression of intestinal detoxification and glutathione biosynthetic enzymes. Cancer Research *61*, 3299–3307.

Moon, J.-S.S., Nakahira, K., Chung, K.-P.P., Nicola, G., Koo, M.J., Pabón, M.A., Rooney, K.T., Yoon, J.-H.H., Ryter, S.W., Stout-Delgado, H., et al. (2016). NOX4-dependent fatty acid oxidation promotes NLRP3 inflammasome activation in macrophages. Nature Medicine *22*, 1002–1012.

Nguyen, T., Nioi, P., and Pickett, C.B. (2009). The Nrf2-antioxidant response element signaling pathway and its activation by oxidative stress. The Journal of Biological Chemistry *284*, 13291–13295.

Odendall, C., Dixit, E., Stavru, F., Bierne, H., Franz, K.M., Durbin, A.F., Boulant, S., Gehrke, L., Cossart, P., and Kagan, J.C. (2014). Diverse intracellular pathogens activate type III interferon expression from peroxisomes. Nature Immunology *15*, 717–726.

Reddy, J., and Hashimoto, T. (2001). Peroxisomal beta-oxidation and peroxisome proliferator-activated receptor alpha: an adaptive metabolic system. Annual Review of Nutrition *21*, 193–230.

Reese, T.A. (2016). Co-infections: Another Variable in the Herpesvirus Latency-Reactivation Dynamic. Journal of virology *90*, JVI.01865-15-5537.

Reese, T., Wakeman, B., Choi, H., Hufford, M., Huang, S., Zhang, X., Buck, M., Jezewski, A., Kambal, A., Liu, C., et al. (2014). Helminth infection reactivates latent γ-herpesvirus via cytokine competition at a viral promoter. Science *345*, 573–577.

Shang, G., Zhang, C., Chen, Z.J., Bai, X.-C.C., and Zhang, X. (2019). Cryo-EM structures of STING reveal its mechanism of activation by cyclic GMP-AMP. Nature *567*, 389–393.

Staels, B., Dallongeville, J., Auwerx, J., Schoonjans, K., Leitersdorf, E., and Fruchart, J. (1998). Mechanism of action of fibrates on lipid and lipoprotein metabolism. Circulation *98*, 2088–2093.

Steed, A.L., Barton, E.S., Tibbetts, S.A., Popkin, D.L., Lutzke, M.L., Rochford, R., and Virgin,

H.W. (2006). Gamma interferon blocks gammaherpesvirus reactivation from latency. Journal of virology *80*, 192–200.

Sychev, Z.E., Hu, A., Dimaio, T.A., Gitter, A., Camp, N.D., Noble, W.S., Wolf-Yadlin, A., and Lagunoff, M. (2017). Integrated systems biology analysis of KSHV latent infection reveals viral induction and reliance on peroxisome mediated lipid metabolism. PLoS pathogens *13*, e1006256.

Teissier, E., Nohara, A., Chinetti, G., Paumelle, R., Cariou, B., Fruchart, J.-C.C., Brandes, R.P., Shah, A., and Staels, B. (2004). Peroxisome proliferator-activated receptor alpha induces NADPH oxidase activity in macrophages, leading to the generation of LDL with PPAR-alpha activation properties. Circulation Research *95*, 1174–1182.

Ye, F., Zhou, F., Bedolla, R.G., Jones, T., Lei, X., Kang, T., Guadalupe, M., and Gao, S.-J.J. (2011). Reactive oxygen species hydrogen peroxide mediates Kaposi's sarcoma-associated herpesvirus reactivation from latency. PLoS Pathogens *7*, e1002054.

You, J., Hou, S., Malik-Soni, N., Xu, Z., Kumar, A., Rachubinski, R.A., Frappier, L., and Hobman, T.C. (2015). Flavivirus Infection Impairs Peroxisome Biogenesis and Early Antiviral Signaling. Journal of Virology *89*, 12349–12361.

Zheng, C., and Su, C. (2017). Herpes simplex virus 1 infection dampens the immediate early antiviral innate immunity signaling from peroxisomes by tegument protein VP16. Virology Journal *14*, 35.

STAR METHODS

Detailed methods are provided in the online version of this paper and include the following:

KEY RESOURCES TABLE

LEAD CONTACT AND MATERIALS AVAILABILITY

EXPERIMENTAL MODEL AND SUBJECT DETAILS

METHOD DETAILS

QIANTIFICATION AND STATISTICAL ANALYSIS

DATA AND CODE AVAILABILITY

KEY RESOURCES TABLE

REAGENT or RESOURCE	SOURCE	IDENTIFIER
Antibodies		
Rabbit monoclonal anti-STING antibody	Cell Signaling	Cat# 13647S; RRID: AB_2732796
Rabbit polyclonal anti-STING antibody	Proteintech	Cat#19851-1-AP; RRID: AB_10665370
Rabbit monoclonal anti-TBK1/NAK antibody	Cell Signaling	Cat# 3504S; RRID: AB_2255663
Rabbit monoclonal anti-Phospho-TBK1 (Ser172) antibody	Cell Signaling	Cat# 5483S; RRID: AB_10693472
Rabbit monoclonal anti-IRF-3 antibody	Cell signaling	Cat# 4302S; RRID: AB_1904036
Rabbit monoclonal anti-Phospho-IRF-3 (Ser396) antibody	Cell Signaling	Cat# 4947S; RRID: AB_823547
Mouse monoclonal anti-SDHA antibody	Abcam	Cat# ab14715; RRID: AB_301433
Mouse monoclonal anti-b-actin antibody	Sigma	Cat# A2228; RRID: AB_476697
Mouse monoclonal anti-PPAR-α antibody	Santa Cruz	Cat# Sc-398394
Rabbit anti-MHV68 polyclonal antibody	Home made	(Weck et al., 1997)
Goat anti-Rabbit IgG(H+L) secondary antibody, Alexa Fluor 647	Thermo Fisher Scientific	Cat# A-21245; RRID: AB_2535813
Donkey anti-Rabbit IgG, Peroxidase	Jackson ImmunoResearch Laboratory	Cat# 711-035-152; RRID: AB_10015282
Goat anti-Mouse IgG, Peroxidase	Jackson ImmunoResearch Laboratory	Cat# 115-035-174; RRID: AB_2338512
Chemicals, Peptides, and Recombinant Proteins		
Fenofibrate	Sigma	Cat# F6020
WY14643	Sigma (In vitro assay); Cayman (In vivo assay)	Cat# C7081; Cat# *50892-23-4*
Rosiglitazone	Sigma	Cat# R2408
GW501516	Sigma	Cat# SML1491
N-Acetyl-L-cysteine	Sigma	Cat# A7250
Hydrogen peroxide solution	Sigma	Cat# 216763
DMXAA	InvivoGen	Cat# tlrl-dmx
2'3'-cGAMP	InvivoGen	Cat# tlrl-nacga23
D-Luciferin, Potassium Salt	GOLDBIO	Cat# LUCK-100
Animal-Free Murine IL-4	PEPROTECH	Cat# AF-214-14
Critical Commercial Assays		
ROS-ID Total ROS detection kit	Enzo	Cat# ENZ-51011
Lipofectamine 3000 Reagent	Thermo Fisher Scientific	Cat# L3000008
Qiagen RNeasy Mini Kit	Qiagen	Cat# 74104
SuperScript VILO cDNA Synthesis Kit	Thermo Fisher Scientific	Cat# 11754050
PowerUp SYBR Green Master Mix	Thermo Fisher Scientific	Cat# A25776
Amplex Red Hydrogen Peroxide/Peroxidase Assay Kit	Thermo Fisher Scientific	Cat# A22188
Mouse IFN Beta ELISA Kit, High Sensitivity	PBL Assay Science	Cat# 42410-1
Deposited Data		
RNA-seq	European Nucleotide Archive	PRJEB33753
Experimental Models: Organisms/Strains		
Mouse: C57BL/6J	The Jackson Laboratory; Bred at UTSW facility with IACUC approval	Stock No. 000664
Mouse: B6;129S4-*Ppar$\alpha^{tm1Gonz}$*/J	The Jackson Laboratory; Bred at UTSW facility with IACUC approval	Stock No. 008154
Mouse: C57BL/6J-*Tmem173^{gt}*/J	The Jackson Laboratory; Bred at UTSW facility with IACUC approval	Stock No. 017537

Mouse: B6(Cg)-*Tmem173*$^{tm1.2Camb}$/J	The Jackson Laboratory; Bred at UTSW facility with IACUC approval	Stock No. 025805
Mouse: B6.129X1-*Nfe2l2*^{tm1Ywk}/J	The Jackson Laboratory; Bred at UTSW facility with IACUC approval	Stock No. 017009
Murine gamma herpesvirus 68(WUSM stain)	ATCC	VR-1465
Murine gamma herpesvirus 68-M3FL	(Hwang et al., 2008)	
Software and Algorithms		
Graphpad Prism 7	GraphPad	www.graphpad.com
FlowJo software	FlowJo	www.flowjo.com
ImageJ Software	NIH	www.imagej.nih.gov/ij/
Ingenuity Pathway Analysis	Ingenuity Systems	www.ingenuity.com
Live Image Software	Perkin Elmer	www.perkinelmer.com

LEAD CONTACT AND MATERIAL AVAILABILITY

Further information and requests for resources and reagents should be directed to and will be fulfilled by the lead contact, Tiffany Reese (tiffany.reese@utsouthwestern.edu). This study did not generate new unique reagents.

EXPERIMENTAL MODELS AND SUBJECT DETAILS

Animals

C57BL/6J, B6;129S4-*Ppar*$\alpha^{tm1Gonz}$/J, C57BL/6J-*Tmem173*^{gt}/J, B6(Cg)-*Tmem173*$^{tm1.2Camb}$/J, B6.129S2-*Ifnar1*^{tm1Agt}/Mmjax, and B6.129X1-*Nfe2l2*^{tm1Ywk}/J were purchased from The Jackson Laboratory. All mice were housed under specific pathogen-free, double-barrier unit at the University of Texas Southwestern Medical Center. Mice were fed autoclaved rodent feed and water. Mice were maintained and used under a protocol approved by UT Southwestern Medical Center Institutional Animal Care and Use Committee (IACUC).

METHOD DETAILS

MHV68 acute replication in mouse

Experiments were carried out using 8-12 weeks old male mice under the protocol approved by IACUC. Mice were injected intraperitoneally with either vehicle control (15% HS15 in normal saline) or WY14643 (100mg/kg) for 1 week starting from 3 days before virus infection. Mice were then infected with MHV68-M3FL at the dose of 10^6 PFU through intraperitoneal route (Hwang et al., 2008; Reese et al., 2014). To quantify virus-encoded luciferase expression, mice

were weighed and injected with 150 mg/kg of D-Luciferin (GOLDBIO) prior to imaging using IVIS Lumina III In Vivo Imaging System (PerkinElmer). Total flux (Photons/second) of the abdominal region was determined using Living Image software (PerkinElmer). Survival of the mice were recorded until 20 days after infection.

MHV68 reactivation in mouse

8-12 weeks old mice were injected intraperitoneally with MHV68-M3FL at the dose of 10^6 PFU (Hwang et al., 2008; Reese et al., 2014). Four weeks after infection, mice were injected with either vehicle control (15% HS15 in normal saline), complex of 5 μg of IL-4 (PEPROTECH) and 25 μg of anti-IL-4 (BioXcell, clone 11B11)(Reese et al., 2014), WY14643 (100 mg/kg) or both IL-4 complex (IL-4c) and WY14643. The reactivation of MHV68 were then quantified by IVIS Lumina III after administration of D-Luciferin.

Cell culture

Bone marrow derived macrophages were differentiated in DMEM with 10% FBS supplemented with 1% glutamine, 1% HEPEs and 10% CMG14 supernatant for 7 days (Reese et al., 2014). 3T12 cells were maintained in DMEM with 5% FBS supplemented with 1% glutamine and 1% HEPES.

Virus infection

Fully differentiated BMDMs were seeded on 24 well plates ($1.5x10^5$ cells per well) or 6 well plate (10^6 cells per well). Cells were pretreated with either vehicle control (0.1% DMSO) or agonists (Fenofibrate 50 μM, WY14643 200 μM, Rosiglitazone 1 μM, GW501516 100 nM) for 16 hours. The next days, macrophages were infected with MHV68 at multiplicity of infection (MOI)=5 or 0.1; cells were infected with MCMV at MOI=1. After an hour, cells were washed with PBS twice to remove unabsorbed viruses and resuspended in medium containing treatments. For growth curve, samples were collected at 0 hour, 24 hours, 48 hours, 72 hours and 96 hours after infection and were frozen at -80 °C. The concentration of virus was titered by plaque assay in 3T12 cells. For flow cytometric analysis cells were collected 24 hours after infection.

Flow cytometry for MHV68 lytic proteins positive cells

To determine the percentage of cells that expressing lytic proteins of MHV68 infection, cells were harvested 24 hours after infection, and fixed with 2% formaldehyde, blocked with 10% mouse serum and 1% Fc block (CD16/32, BioLegend), then stained with polyclonal rabbit

antibody to MHV68 (1:1000) (Reese et al., 2014; Weck et al., 1997), followed by secondary goat anti-rabbit Alexa Fluor-647 (Invitrogen).

Transfection

Cells were seeded on 6 well plates and treated as needed. Cells were transfected with STING ligand (DMXAA, 10 μg/ml, InvivoGen) using Lipofectamine 3000 (Thermo Fisher Scientific) according to the manufacturer's protocol.

Plaque assay

The concentration of virus was titered in 3T12 cells. The frozen samples containing viruses were thawed in incubator, the serial diluted samples were then added on the monolayer of 3T12 cells. After an hour of absorption, the cells were then covered with 1% methylcellulose. Plates were incubated at 37 °C for 7 days, and the plaques were stained with 0.1% crystal violet.

Western blot

Cells were lysed with RIPA buffer (150 mM NaCl, 1% NP-40, 0.5% sodium deoxycholate, 0.1% SDS, 25 mM Tris with protease inhibitor cocktail). Protein concentration were determined using Bradford assay (Bio-Rad). Equal amounts of protein were resolved by SDS-PAGE, transferred to nitrocellulose membrane, immunoblotted with specific primary and secondary antibodies, and developed using Luminata Forte Western HRP substrate (Millipore).

QRT-PCR

BMDMs in 6 well plates were either infected with MHV68 at MOI=5 for 6 hours or transfected with STING ligand DMXAA at 10 μg/ml for 2 hours. RNA was extracted using Qiagen RNeasy Mini Kit (Qiagen) and reverse transcribed into cDNA using SuperScript VILO cDNA Synthesis Kit (Invitrogen). Relative quantification of target genes was determined using PowerUp SYBR Green Master Mix in a QuantStudio 7 Flex real time PCR system.

IFNβ ELISA Assay

BMDMs were seeded in 24 well plates, the next day, cells were treated with either vehicle control or WY14643 for 16 hours. Cells were then transfected with DMXAA at the concentration of 10 μg/ml. Supernatant of cells were collected at 24 hours after transfection and frozen at -80 °C. The concentration of IFNβ in the supernatant was determined with PBL IFN Beta ELISA Kit (PBL Assay Science).

Total ROS measurement

The total ROS production was determined using ROS-ID Total ROS detection kit (Enzo) according to the manufacture's protocol. Cells were seeded on 24 well plates, and treatment with indicated compounds or DMSO as vehicle control for 6 hours, followed by incubation with oxidative stress detection reagent for 30 mins at 37 °C. The fluorescence of the detection reagent upon oxidation was analyzed by flow cytometry using a FACSCalibur (BD Biosciences).

RNA seq and data analysis

RNA samples were extracted with RNeasy Mini Kit (Qiagen) and RNA library was prepared using TruSeq Stranded mRNA Sample Preparation Kit (Illumina). Samples were sequenced on NextSeq 500/500 sequencer (Illumina) with SE-85. RNA seq data is normalized and analyzed based on the use of "internal standards" (Rocke and Durbin, 2001) that characterize some aspects of the system's behavior, such as technical variability, as presented elsewhere (Dozmorov and Centola, 2003; Dozmorov and Lefkovits, 2009). The two-step normalization procedure and the Associative analysis functions are implemented in MATLAB (MathWorks, MA) and available from authors upon request. Functional analysis of identified genes was performed with Ingenuity Pathway Analysis (IPA; Ingenuity System). The sequencing data has been deposited in the European Nucleotide Archive under the accession number PRJEB33753.

QUANTIFICATION AND STATISTICAL ANALYSIS

All data are presented as mean ± SD. Statistical comparisons were performed using Graphpad Prism 7.0 software. Data were compared using unpaired two-tailed t test, one-way or two-way ANOVA. Statistical significance was set at $p < 0.05$. The numbers of independent replicates (n) are reported in the figure legends.

REFERENCES

Dozmorov, I., and Centola, M. (2003). An associative analysis of gene expression array data. Bioinformatics (Oxford, England) *19*, 204–211.

Dozmorov, I., and Lefkovits, I. (2009). Internal standard-based analysis of microarray data. Part 1: analysis of differential gene expressions. Nucleic Acids Research *37*, 6323–6339.

Hwang, S., Wu, T.-T., Tong, L.M., Kim, K., Martinez-Guzman, D., Colantonio, A.D., Uittenbogaart, C.H., and Sun, R. (2008). Persistent gammaherpesvirus replication and dynamic interaction with the host in vivo. Journal of virology *82*, 12498–12509.

Reese, T., Wakeman, B., Choi, H., Hufford, M., Huang, S., Zhang, X., Buck, M., Jezewski, A., Kambal, A., Liu, C., et al. (2014). Helminth infection reactivates latent γ-herpesvirus via cytokine competition at a viral promoter. Science *345*, 573–577.

Rocke, D., and Durbin, B. (2001). A model for measurement error for gene expression arrays. Journal of Computational Biology : A Journal of Computational Molecular Cell Biology *8*, 557–569.

Weck, K.E., Canto, A.J., Gould, J.D., O'Guin, A.K., Roth, K.A., Saffitz, J.E., Speck, S.H., and Virgin, H.W. (1997). Murine γ-herpesvirus 68 causes severe large-vessel arteritis in mice lacking interferon-γ responsiveness: A new model for virus-induced vascular disease. Nature medicine *3*, 1346–1353.

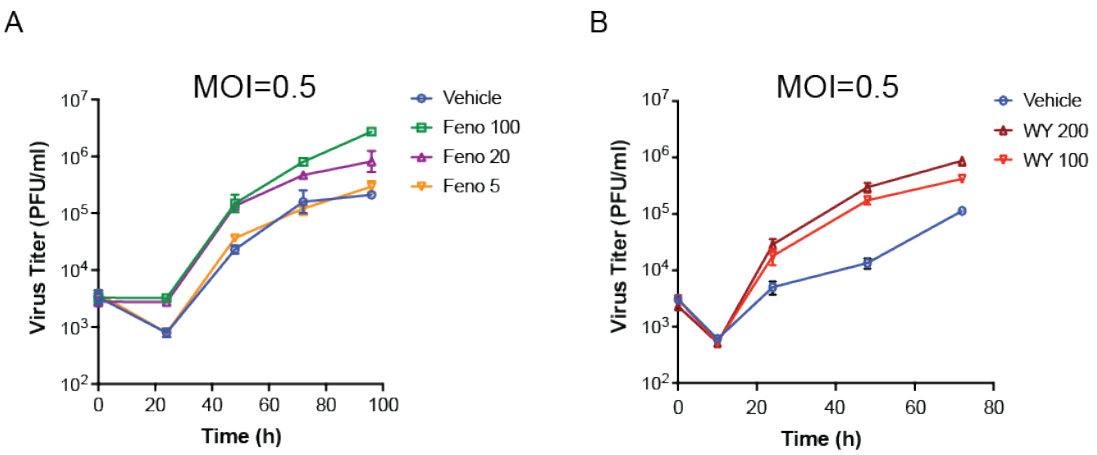

Supplemental Figure 1. Viral replication with different doses of fenofibrate and WY14643.

(A) Macrophages from C57BL6/J mice were treated with vehicle or increasing doses of fenofibrate (5, 20, or 100 μM) for 16 hours. Cells were infected with MHV68 at MOI=0.5 and viral growth was quantitated by plaque assay on 3T12 cells.

(B) Macrophages from C57BL6/J mice were treated with vehicle or increasing doses of WY14643 (100 or 200 μM) for 16 hours. Cells were infected with MHV68 at MOI=0.5 and viral growth was quantitated by plaque assay on 3T12 cells.

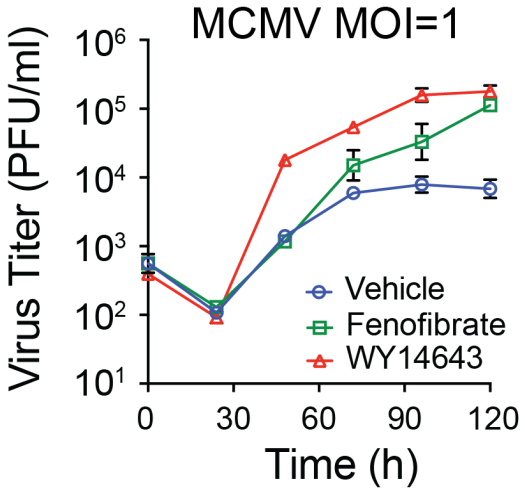

Supplemental Figure 2. PPAR-α stimulation increases virus replication of MCMV.

Growth curve of MCMV in macrophages isolated from C57BL/6J mice after pretreatment with vehicle, WY14643 or fenofibrate. Cells were infected with MCMV at MOI=1. Data represents mean ± SD from 2 independent experiments.

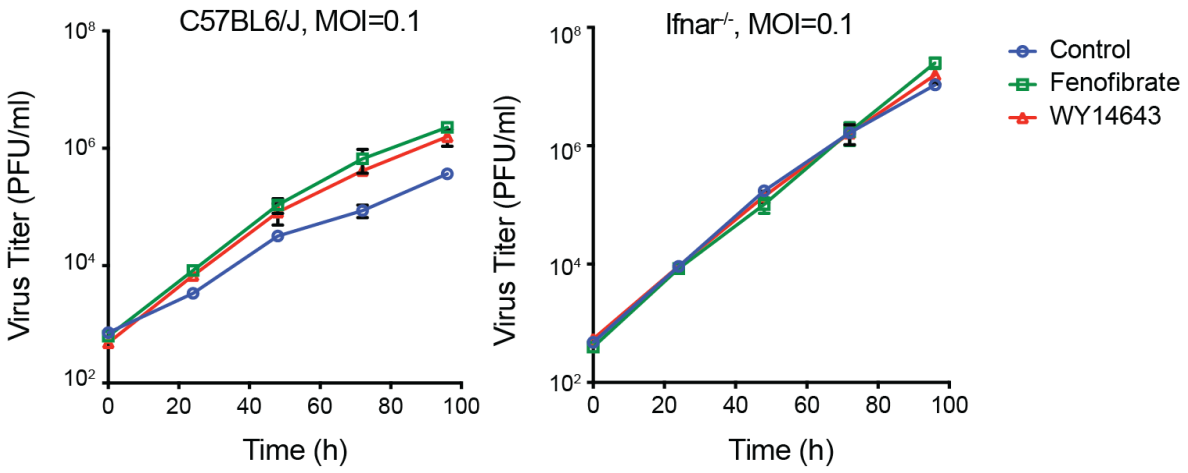

Supplemental Figure 3. Effects of PPAR-α stimulation are IFNAR-dependent.

Macrophages from C57BL6/J mice or *Ifnar*$^{-/-}$ mice were treated with vehicle, fenofibrate or WY14643 for 16 hours. Cells were infected with MHV68 at MOI=0.1 and viral growth was quantitated by plaque assay on 3T12 cells.

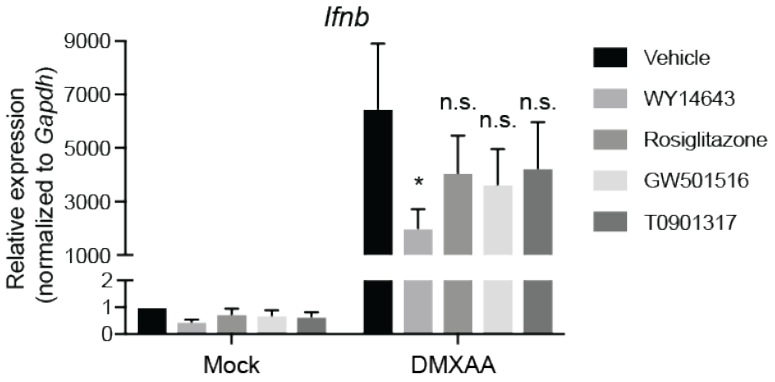

Supplemental Figure 4. *Ifnb* expression after treatment with PPAR-α, PPAR-γ, PPAR-δ, or LXR-α agonists. Macrophages from C57BL6/J mice were treated with vehicle, WY14643, rosiglitazone, GW501516, or T0901319 for 16 hours. Cells were then transfected with DMXAA and *Ifnb* expression was quantitated from lysates 2 hours after transfection. Expression was normalized to *Gapdh*. Data all shown as mean ± SD; $^{*}p<0.05$, n.s. (not significant), relative to DMXAA/vehicle treated. Statistical analysis was conducted using two-way ANOVA test.

Table 1. Differential expression of genes involved in innate inflammatory response

Gene	Mock			WY14643			MHV68			MHV68+WY14643			cGAS	PRR	NF-κB Signaling	IL-6 Signaling	Interferon Signaling	Acute Phase Response Signaling
	1	2	3	1	2	3	1	2	3	1	2	3						
IL18	214	181	177	166	184	187	2342	2438	1992	1720	1678	1694		√	√	√		√
TNF	1498	1498	2067	906	880	922	7828	7552	9224	2083	2178	2160		√	√	√		√
NFKBIE	1115	1114	1425	710	718	658	4615	4386	4872	1432	1454	1466		√	√	√		√
IL1RN	1340	1545	1464	547	527	514	5950	5147	5320	1755	1690	1957		√	√	√		√
IL1A	2	5	4	2	1	4	11	12	7	7	5	6		√	√	√		√
NFKBIB	1048	993	1001	701	639	693	2365	2360	2255	1204	1170	1239		√	√	√		√
NFKBID	467	454	580	579	581	587	1015	987	1250	638	761	644		√	√	√		√
TRAF2	645	642	665	534	543	561	1418	1407	1315	723	682	758		√	√	√		√
FGFR1	26	33	16	51	45	49	57	46	71	133	111	130		√	√	√		
PIK3R6	428	466	500	472	503	433	993	880	1068	690	669	631		√	√	√		
MYD88	2254	2195	2088	1965	2059	2004	9418	9895	9174	5842	5502	5838		√	√			√
TLR3	421	427	444	378	340	355	10029	8707	11218	5054	5306	5146		√	√			
EIF2AK2	1538	1482	1706	1108	1144	1171	12635	11494	14915	10992	10945	10909		√	√			
TLR2	10294	9509	11192	4098	4381	4192	32293	32202	32585	10216	9579	10529		√	√			
CASP8	2315	2384	2334	2862	2842	2834	6680	6252	6824	5428	5339	5493		√	√			
TNFSF13B	38	31	33	15	24	21	126	72	71	46	43	47		√	√			
TLR7	5389	5467	5714	3498	3413	3314	14199	12773	16330	9071	9016	9201		√	√			
TLR9	531	562	595	428	462	391	1478	962	1968	698	677	666		√	√			
TANK	1682	1676	1782	1158	1102	1181	4226	4062	4476	1977	1885	1965		√	√			
TLR8	3210	3237	3607	4598	4490	4216	7612	6779	9623	9866	9657	9574		√	√			
TLR6	469	466	455	461	421	416	974	867	987	703	601	687		√	√			
IL6	0	1	0	0	0	0	17	19	12	0	0	1		√		√		√
IKBKE	2727	2630	3106	2355	2312	2210	5996	5642	6981	3036	3082	3026		√		√		√
RASD2	6	6	5	6	4	3	10	10	16	6	6	10		√		√		√
IFNB1	1	1	0	0	0	0	44	34	35	1	0	5		√			√	
OAS3	1140	1141	1375	423	432	472	20896	17992	24239	17435	18349	17669		√			√	
OAS1G	189	233	200	82	89	104	3479	3341	3363	2206	2189	2223		√			√	
OAS1B	67	76	85	62	58	57	991	970	1181	640	774	728		√			√	
OAS1A	1021	1027	1007	453	448	473	11361	11963	10270	8194	7779	8206		√			√	

Gene	Mock			WY14643			MHV68			MHV68+WY14643			cGAS	PRR	NF-κB Signaling	IL-6 Signaling	Interferon Signaling	Acute Phase Response Signaling
	1	2	3	1	2	3	1	2	3	1	2	3						
OAS1C	117	111	92	86	77	74	798	912	774	578	581	601		√			√	
OAS2	756	766	1041	554	522	606	6160	4675	8929	5527	7345	5504		√			√	
C3	1174	1109	1159	479	499	448	13193	11612	15130	3365	3258	3503		√				√
TNFSF10	57	38	77	6	7	3	8736	8454	9395	3696	3442	3747		√				
CCL5	81	72	49	16	18	10	4182	4011	3520	437	368	437		√				
IRF7	772	815	783	150	173	159	41147	40260	40824	26639	26479	27343		√				
IFIH1	779	753	843	440	492	461	19733	19001	21380	11666	11350	11898		√				
TNFSF4	18	13	11	31	41	34	336	235	296	206	173	209		√				
DDX58	1163	1235	1444	624	600	595	22888	21147	26983	18054	18158	17569		√				
TNFSF15	11	14	7	3	3	4	181	180	208	39	38	37		√				
DHX58	914	946	913	474	423	431	14302	14384	14283	10439	10498	10630		√				
IL15	383	365	330	343	318	303	4611	5055	4337	2110	1883	2100		√				
TNFSF8	105	100	104	27	35	41	1236	1072	1240	442	470	499		√				
NOD1	270	264	288	308	303	294	2845	2959	3223	1535	1358	1616		√				
PRKCE	11	15	19	19	21	22	133	96	155	100	86	99		√				
TRAF1	150	168	186	71	73	77	1306	1071	1148	199	181	216		√				
NOD2	186	207	205	175	137	139	1270	1130	1498	584	502	521		√				
IL10	37	38	30	26	24	21	172	198	185	63	58	78		√				
CASP1	2087	2038	2095	1881	1871	1987	10078	10059	9223	6595	6505	6608		√				
RIPK2	488	508	503	397	450	428	1906	1971	2007	1025	868	990		√				
TRIM25	2609	2607	2681	3196	3243	3160	8390	7793	9505	7358	7478	7335		√				
IRAK2	1569	1516	1703	1172	1144	1118	4749	4796	4977	2506	2407	2619		√				
LTB	6	3	10	7	8	9	13	16	18	13	9	11		√				
UBC	1912	1952	2446	2259	2271	2144	5354	5568	4599	4788	4751	4965		√				
RELB	1280	1279	1423	643	676	648	2960	2877	3028	1235	1319	1394		√				
AKT3	1145	1188	1307	1350	1403	1392	4945	4111	5354	3544	3477	3528			√	√		√
TNFRSF1B	11046	10749	11198	11923	12072	11725	26748	24892	26938	21453	20583	22081			√	√		√
RAF1	2717	2725	2818	2829	2810	2989	5410	5632	5480	3984	3973	3967			√	√		√
IL1R2	16	20	17	6	8	11	46	64	48	48	24	44			√	√		
STAT3	2636	2581	2720	2997	3128	3133	6711	6102	7306	5448	5229	5591			√			√
FLT4	6	6	5	7	5	5	298	219	257	141	155	168			√			

Gene	Mock			WY14643			MHV68			MHV68+WY14643			cGAS	PRR	NF-κB Signaling	IL-6 Signaling	Interferon Signaling	Acute Phase Response Signaling
	1	2	3	1	2	3	1	2	3	1	2	3						
CD40	241	224	225	52	66	58	8145	8503	7354	2111	2001	2282			√			
KDR	459	502	491	158	190	167	6428	5838	7733	2610	2305	2611			√			
LCK	3	8	8	7	5	10	71	69	63	50	34	41			√			
FLT1	180	190	199	146	128	136	1388	1091	1428	737	675	603			√			
AZI2	1206	1171	1153	1122	1104	1165	5505	5316	5657	4208	4033	4081			√			
PELI1	1274	1231	1252	1057	1012	1060	5312	5420	5837	2669	2403	2658			√			
BMP2	24	23	21	5	5	7	70	76	109	22	8	16			√			
TNFAIP3	1394	1344	1533	743	713	674	4082	3777	4771	1402	1368	1419			√			
MAP3K8	248	238	255	321	312	290	615	625	660	430	407	464			√			
HDAC1	1141	1145	1196	1066	1040	1061	2699	2781	2588	1917	1923	1980			√			
SOCS1	28	33	30	23	20	14	953	1044	901	287	235	264				√	√	√
JAK2	919	925	1001	904	962	953	7304	6852	7891	4262	4168	4193				√	√	√
SOCS3	161	147	181	75	87	72	768	793	919	165	180	159				√	√	
CEBPB	1690	1677	1865	1568	1350	1260	5033	5023	5532	3049	3278	3081				√		√
IL1RAP	243	249	254	275	260	287	762	704	721	708	756	757				√		√
MAP2K1	4735	4703	4591	4638	4544	4542	11578	11466	11049	10140	9435	9856				√		√
TNFAIP6	0	1	0	1	1	1	20	18	5	6	2	8				√		
MCL1	13370	13145	14265	10744	10256	10032	36309	36405	37898	21989	22645	22945				√		
MAPKAPK2	7602	7229	7788	5230	5062	5124	19231	19768	19006	9309	9084	9768				√		
IL18RAP	93	98	81	127	129	132	183	173	200	114	92	111				√		
IFIT3	699	752	718	68	83	84	71547	76452	75258	52105	48862	51428					√	
ISG15	467	442	412	69	63	68	32503	34593	29861	18088	17179	18568					√	
STAT1	4405	4219	4528	2076	2201	2115	58462	59483	63427	49801	48886	49545					√	
TAP1	1796	1669	1594	1130	1211	1121	19657	20391	19816	13324	12700	13429					√	
IFI35	864	872	808	516	589	578	9556	10614	8826	6491	6282	6391					√	
STAT2	2294	2150	2473	2140	2086	2029	23292	21943	27767	21528	22535	21756					√	
IRF1	1456	1280	1410	877	902	870	9931	10321	11085	3871	3612	4169					√	
PSMB8	2270	2208	2023	1597	1730	1617	12367	13142	11161	8068	7882	8075					√	
IFITM3	6415	6793	6129	2309	2653	2393	28056	28253	24744	17039	16637	17767					√	
SOCS7	549	559	534	639	607	542	1951	1755	2336	998	969	1025					√	

Gene	Mock			WY14643			MHV68			MHV68+WY14643			cGAS	PRR	NF-κB Signaling	IL-6 Signaling	Interferon Signaling	Acute Phase Response Signaling
	1	2	3	1	2	3	1	2	3	1	2	3						
IRF9	1419	1387	1584	1027	977	1001	3698	3583	3662	3237	3324	3305					√	
TYK2	2458	2323	2598	2846	2750	2779	5953	4969	6582	4094	4265	4089					√	
CFB	49	57	51	30	35	43	1543	1481	1338	365	396	389						√
SOCS2	6	7	19	9	9	9	128	121	127	35	27	45						√
CP	68	62	72	30	30	20	458	372	441	70	82	70						√
C2	6	7	5	3	9	7	40	31	33	18	34	23						√
C1RA	59	64	44	32	32	26	232	191	202	87	98	108						√
HP	6	9	9	3	0	2	30	31	22	7	7	3						√
F8	10	10	9	9	4	3	28	38	32	15	15	8						√
TCF4	2157	2046	2139	2014	1969	1919	5627	5273	6623	3476	3550	3464						√
HMOX2	2103	2139	2025	1688	1745	1845	5653	5928	5272	4839	4635	4826						√
APOA2	4	7	3	5	4	1	11	11	8	7	4	5						√
NFKBIA	3201	3134	3526	2777	2672	2730	9695	10176	10278	4679	4668	4725	√	√	√	√		√
CASP12	3	2	1	0	1	0	41	41	44	16	16	13	√					
CASP4	403	346	464	201	202	221	4588	4483	4288	1987	1950	2141	√					
TREX1	1147	1150	1174	674	642	620	11338	12083	10822	6742	6376	7018	√					
SQSTM1	17196	16704	18097	24329	24385	23906	33074	33293	32163	36959	35126	37671	√					
TBK1	2377	2384	2397	2445	2400	2397	4357	4293	4487	3062	3230	3201	√					
CHUK	1441	1529	1573	1640	1608	1568	2029	1945	2083	1871	1823	1826	√					
MAP1LC3A	429	391	455	525	461	523	579	585	491	515	521	499	√					
BAX	3470	3327	3128	3226	3204	3212	4116	4459	3952	3809	3902	3871	√					
RPS6KB1	787	790	857	979	1006	968	779	752	875	834	863	832	√					
IRF3	1127	1158	1171	1314	1318	1297	1056	1150	1135	1128	1193	1141	√					
ULK1	976	933	1021	1419	1423	1376	550	451	674	913	881	831	√					

List of genes and their expression values across three biological replicates for each of the four groups (Vehicle-treated, WY14643-treated, MHV68-infected, and MHV68-infected/WY14643-treated). Membership of genes in various inflammatory pathways as defined by Ingenuity are listed.

Table 2. Differential expression of genes involved in cellular oxidative stress with WY14643 treatment

Gene	Mock			WY14643			Redox Metabolism	Iron Metabolism	Nrf2-Mediated Oxidative Stress	Antioxidant action of vitamin C
	1	2	3	4	5	6				
Txnrd1	4828	5101	4918	14630	14375	15191	√		√	
Cat	769	791	692	1777	1761	1810	√		√	
Gsr	9	16	11	92	97	96	√		√	
Gsta3	2029	2066	2272	4601	4581	4414	√		√	
Gstm1	26	27	13	35	46	46	√		√	
Gstp1	52	61	63	102	115	94	√		√	
Gstt2	1153	1030	1088	2740	2838	2751	√		√	
Mgst1	46	61	57	149	173	146	√		√	
Nqo1	25451	25969	25176	41463	42096	44113	√		√	
Prdx1	2764	2846	2704	4726	4787	4796	√		√	
Sod1	1529	1507	1545	2365	2413	2522	√		√	
Prdx6	171182	175383	170069	318219	297781	303528	√			
Ftl1	395	374	413	845	866	738		√	√	
Gdf15	3463	3641	3357	8580	8300	8575		√		
Slc11a1	1521	1513	1711	2765	2739	2793		√		
Slc25a37	3312	3349	2766	10243	10169	9856		√		
Slc40a1	7171	7229	7051	11446	11255	11091		√		
Slc48a1	23341	23271	21494	55598	51879	54662		√		
Hmox1	1514	1553	1775	3111	2875	2869			√	√
Fos	6	11	18	22	20	23			√	
Prkcg	4600	4834	4718	7321	7279	7459			√	
Abcc1	4	4	5	20	21	20			√	
Aox1	27	33	27	113	101	113			√	
Dnajb13	1735	1782	1732	3403	3358	3463			√	
Gclc	2141	2187	2058	7881	7657	8343			√	
Gclm	1757	1677	1801	2744	2639	2745			√	
Ikbkg	26	25	28	43	46	57				√
Abhd3	2762	2689	2970	5391	5051	5302				√

Gene	Mock			WY14643			Redox Metabolism	Iron Metabolism	Nrf2-Mediated Oxidative Stress	Antioxidant action of vitamin C
	1	2	3	4	5	6				
Csf2ra	807	791	741	1746	1631	1595				√
Pla2g7	7	6	7	2	3	0				√
Plb1	37	33	44	21	26	21				√
Pla2g2e	1498	1498	2067	906	880	922				√
Tnf	270	254	299	185	169	194				√
Plcb4	1115	1114	1425	710	718	658				√
Nfkbie	2674	2553	3021	1835	1808	1725				√
Nfkb2	839	915	987	106	128	149				√
Rsad2	248	241	250	141	128	122			√	
Maff	2481	2269	2687	1394	1483	1347			√	
Herpud1	126	152	112	85	64	69			√	
Acta2	6	9	9	3	0	2		√	√	
Hp	68	62	72	30	30	20		√		
Cp	7	9	8	3	4	1				
Sod3	4828	5101	4918	14630	14375	15191	√		√	

List of genes and their expression values across three biological replicates for vehicle-treated and WY14643-treated groups. Membership of genes in various oxidative stress pathways as defined by Ingenuity are listed.